Investigation of the variations in the water leaving polarized reflectance from the POLDER satellite data over two biogeochemical contrasted oceanic areas.

Hubert Loisel[1], Lucile Duforet[1], David Dessailly[1], Malik Chami[2], and Philippe Dubuisson[3]

[1]*Université du Littoral Côte d'Opale, Laboratoire d'Océanologie et de Géosciences, 62930 Wimereux, France*
[2]*Université Pierre et Marie Curie-Paris6, Laboratoire Océanographie de Villefranche, 06230 Villefranche sur Mer, France*
[3]*Université de Lille 1, Laboratoire d'Optique Atmosphérique, 59655 Villeneuve d'Ascq cedex, France*

Abstract: The biogeochemical characterization of marine particles suspended in sea water, is of fundamental importance in many areas of ocean science. Previous studies based on theoretical calculations and field measurements have demonstrated the importance of the use of the polarized light field in the retrieval of the suspended marine particles properties. However, because of the weakness of the water leaving polarized signal and of the limited number of appropriate spatial sensors, such measurements have never been exploited from space. Here we show that the marine polarized remote sensing reflectance, as detected from the POLarization and Directionality of the Earth's Reflectances (POLDER) sensor, can be measured from space over bright waters and in absence of aerosols. This feasibility study is carried out over two oceanic areas characterized by different nature of the bulk particulate assemblage: the Barents sea during an intense coccolithophore bloom, and the Rio de la Plata estuary waters dominated by suspended sediments. The retrieved absolute values of the degree of polarization, *P*, its angular pattern, and its behavior with the scattering level are consistent with theory and field measurements. Radiative transfer simulations confirm the sensitivity of the POLDER-2 *P* values to the nature of the particulate assemblage. These preliminary results are very promising for the assessment of the bulk particle composition from remote sensing of the polarized signal, at least over highly scattering waters.

OCIS codes: (120.0280) Remote sensing and sensors; (010.0010) Atmosphere and ocean optics; (260.5430) Polarization; (010.5620) Radiative transfer.

References and links

1. IOCCG (2006), "Remote sensing of inherent optical properties: Fundamentals, tests of algorithms, and applications, in Reports of the International Ocean Colour Coordinating Group," Z. -P. Lee ed., Reports of the International Ocean-Colour Coordinating Group, No. 5, IOCCG, Dartmouth, Canada. (Available at http://www.IOCCG.org/groups/OCAG_data.html).
2. D. Stramski, R. A. Reynolds, M. Kahru, and B. G. Mitchell, "Estimation of particulate organic carbon in the ocean from satellite remote sensing," Science **285**, 239-242 (1999).
3. H. Loisel, E. Bosc, D. Stramski, K. Oubelker, and P.-Y. Deschamps, "Seasonal variability of the backscattering coefficients in the Mediterranean Sea based on Satellite SeaWIFS imagery," Geophys. Res. Lett. **28**, 4203-4206 (2001).
4. M. Stramska and D. Stramski, "Variability of particulate organic carbon concentration in the north polar Atlantic based on ocean color observations with Sea-viewing Wide Field-of-view Sensor (SeaWiFS)," J. Geophys. Res. **110**, C10018, doi:10.1029/2004JC002762 (2005).

#94370 - $15.00 USD Received 28 Mar 2008; revised 22 May 2008; accepted 12 Jun 2008; published 11 Aug 2008

5. H. Loisel, J. M. Nicolas, P.-Y. Deschamps, and R. Frouin, “Seasonal and inter-annual variability of the particulate matter in the global ocean,” Geophys. Res. Lett. **29** (2002).
6 D. A. Siegel, S. Maritorena, N. B. Nelson, D. A. Hansell, and M. Lorenzi-Kayser, “Global distribution and dynamics of colored dissolved and detrital organic materials,” J. Geophys. Res. **107**, 3228, doi:10.1029/2001JC000965 (2002)
7. H. Loisel, J. M. Nicolas, A. Sciandra, D. Stramski, and A. Poteau, "Spectral dependency of optical backscattering by marine particles from satellite remote sensing of the global ocean,” J. Geophys. Res **111**, C09024, doi:10.1029/2005JC003367 (2006).
8. S. Alvain, C. Moulin, Y. Dandonneau, and F.-M. Bréon, “Remote sensing of phytoplankton groups in case 1 waters from global SeaWiFS imagery,” Deep-Sea Research Part I – Instruments and Methods **52**, 1989–2004 (2005).
9. T. K. Westberry and D. A. Siegel, “Spatial and temporal distribution of *Trichodesmium* blooms in the world's oceans,” in *Global Biogeochemical Cycles* **20**, GB4016, doi:10.1029/2005GB002673 (2006)
10. J. Uitz, H. Claustre, A. Morel, and A. S. Hooker, “Vertical distribution of phytoplankton communities in open ocean: an assessment based on surface chlorophyll,” J. Geophys. Res. **111**, C08005, doi:10.1029/2005JC003207 (2006).
11. A. M. Ciotti and A. Bricaud, “Retrievals of a size parameter for phytoplankton and spectral light absorption by colored detrital matter from water-leaving radiances at SeaWiFS channels in a continental shelf region off Brazil,” Limnol. Oceanogr. **4**, 237–253 (2006).
12. A. Ivanoff, N. Jerlov, and T. H. Waterman, “A comparative study of irradiance, beam transmittance and scattering in the sea near Bermuda,” Limnol. Oceanogr. **6**, 129-148 (1961).
13. G. F. Beardsley, “Mueller scattering matrix of sea water,” J. Opt. Soc. Am. **58**, 52-57 (1968).
14. K. J. Voss and E. S. Fry, “Measurement of the Mueller matrix for ocean water,” Appl. Opt. **23**, 4427-4439 (1984).
15. M. Chami and D. McKee, “Determination of biogeochemical properties of marine particles using above water measurements of the degree of polarization at the Brewster angle,” Opt. Express **15**, 9494-9509 (2007).
16. G.W. Kattawar, “Polarization of light in the ocean,” in *Ocean Optics*, R.W. Spinrad, K. L. Carder and M. J. Perry eds. (Oxford University Press, New York), pp. 202-225 (1994).
17. P. C. Y. Chang, J. G. Walker, E. Jakmeman, and K. I. Hopcraft, “Polarization properties of light multiply scattered by non-spherical Rayleigh particles,” Wav. Rand. Med. **9**, 415-426. (1999).
18. M. Chami, R. Santer, and E. Dilligeard, "Radiative transfer model for the computation of radiance and polarization in an ocean-atmosphere system: polarization properties of suspended matter for remote sensing," Appl. Opt. **40**, 2398-2416 (2001).
19. J. Chowdhary, B. Cairns, and L. D. Travis, "Contribution of water-leaving radiances to multiangle, multispectral polarimetric observations over the open ocean: bio-optical model results for case 1 waters," Appl. Opt. **45**, 5542-5567 (2006).
20. M. Chami, "Importance of the polarization in the retrieval of oceanic constituents from the remote sensing reflectance," J. Geophys. Res. **112** (2007).
21. M. Chami and M. Defoin-Platel, “Sensitivity of the retrieval of the inherent optical properties of marine particles in coastal waters to the directional variations and the polarization of the reflectance,” J. Geophys. Res. **112**, C05037, doi:10.1029/2006JC003758 (2007).
22. J. L. Deuzé, F.-M. Bréon, C. Devaux, P. Goloub, M. Herman, B. Lafrance, F. Maignan, M. Marchand, F. Nadal, G. Perry, and D. Tanré, “Remote sensing of aerosols over land surfaces from POLDER-ADEOS-1 polarized measurements,“ J. Geophys. Res. **106,** 4913-4926 (2001).
23. J. Chowdhary, B. Cairns, and L. D. Travis, "Case studies of aerosol Retrievals over the ocean from multiangle, multispectral photopolarimetric remote sensing data," J. Atmos. Sci. **59**, 383-397 (2002).
24. P. Goloub, M. Herman, M. Chepfer, J. Riedi, G. Brogniez, P. Couvert, and G. Sèze, “Cloud thermodynamical phase classification from the POLDER aspaceborn instrument,” J. Geophys. Res. **105**, 14747-14759 (2000).
25. T. Harmel and M. Chami, “Invariance of polarized reflectance measured at the top of atmosphere by PARASOL satellite instrument in the visible range with marine constituents in open ocean waters,” Opt. Express **16**, 6064-6080 (2008).
26. P. Y. Deschamps, F.-M. Breon, M. Leroy, A. Podaire, A. Bricaud, J. C. Buriez, and G. Seze, "The Polder Mission - Instrument Characteristics And Scientific Objectives," IEEE Trans. Geosci. Remote Sens. **32**, 598-615 (1994).
27. J. E. Hansen and L. D. Travis, “Light scattering by planetary atmosphere,” Space Sci. Rev. **16**, 527-610 (1974).
28. A. Ivanoff and T. H. Waterman, “Factors, mainly depth and wavelength, affecting the degree of underwater light polarization,” J. Mar. Res. **16**, 283-307 (1958).
29. T. H. Waterman, “Polarization patterns in submarine illumination,” Science **120**, 927-932 (1954).
30. T. H. Waterman, “Polarized light and plankton navigation,” in *Perspective in Marine Biology*, A. A. Buzzati-Traverso, ed. (University of California Press, Berkley, 1958).
31. A. Morel, "Diffusion de la lumière par les eaux de mer: Resultats expérimentaux et approche théorique," in *Optics of the Sea AGARD Lecture Ser.* **61**, (North Atlantic Treaty Org., Brussels) pp. 3.1.1–3.1.76 (1973).

#94370 - $15.00 USD Received 28 Mar 2008; revised 22 May 2008; accepted 12 Jun 2008; published 11 Aug 2008

32. G. F. Beardsley, "Mueller scattering matrix of sea water," J. Opt. Soc. Am. **58**, 52-57 (1968).
33. A. Lerner, E-H. Carynelisa, S. Nadav, and S. Shai, "On the Quest for the Scattering Mechanism that Determines the Polarization," presented at the Ocean Optics Meeting XVIII, Montreal, Canada (2007).
34. D. A. Siegel, M. Wang, S. Maritorena, and W. Robinson, "Atmospheric correction of satellite ocean color imagery: the black pixel assumption," Appl. Opt. **39**, 3582-3591 (2000).
35. K. G. Ruddick, V. De Cauwer, Y. J. Park, and G. Moore, "Seaborne measurements of near infrared water-leaving reflectance: the similarity spectrum for turbid waters," Limnol. Oceanogr. **51**, 1167-1179 (2006).
36. L. Duforet**,** P. Dubuisson, and R. Frouin. 2007, "Importance and estimation of aerosol vertical structure in satellite ocean-color remote sensing," Appl. Opt. **46**, 1107-1119 (2007).
37. C. Cox and W. Munk, "Measurements of the roughness of the sea surface from photographs of the sun's glitter," J. Opt. Soc. Am. **44,** 838–850 (1954).
38. G. Kattawar and C. Adams, "Stokes vector calculations of the submarine light field in an atmosphere-ocean with scattering according to Rayleigh phase matrix," Limnol. Oceanogr. **34**, 1463-1472 (1989).
39. H. R. Gordon and T. Du, "Light scattering by nonspherical particles: application to coccoliths detached from *Emiliania huxleyi*," Limnol. Oceanogr. **46,** 1438–1454. (2001).
40. R. M. Pope and E. S. Fry, "Absorption spectrum (380-700 nm) of pure water.2. Integrating cavity measurements," Appl. Opt. **36**, 8710-8723 (1997).
41. J. L. Laborde and G. J. Nagy, "Hydrography and sediments transport characteristics of the Río de la Plata a review," in *Estuaries of South America*, G. M. E. Perillo, M. C. Piccolo, and M. Pino Quivira, eds. (Springer, Berlin, 1999), pp. 133–159.
42. D. Doxaran, N. Cherukuru, and S. J. Lavender, "Apparent and inherent optical properties of turbid estuarine waters: measurements, empirical quantification relationships, and modeling, " Appl. Opt. **45**, 2310-2324 (2006).
43. "Analyse Mission de l'impact des non-conformités mesurées sur l'instrument POLDER," Rapport du groupe mission POLDER CNES-DPI /TL/96-004 (1996).
44. W. M. Balch, K. Kilpatrick, P. M. Holligan, D. Harbour, and E. Fernandez, "The 1991 coccolithophore bloom in the central north Atlantic II: relating optics to coccolith concentration," Limnol. Oceanogr. **41,** 1684–1696 (1996).
45. T. J. Smyth, T. Tyrrell, and B. Tarrant, "Time series of coccolithophore activity in the Barents Sea, from twenty years of satellite imagery," Geophys. Res. Lett. **31**, L11302, doi:10.1029/2004GL019735 (2004).
46. H. Siegel, T. Ohde, M. Gerth, G. Lavik, and T. Leipe, "Identification of coccolithophore blooms in the SE Atlantic Ocean off Namibia by satellites and in-situ methods," Cont. Shelf Res. **27**, 258-274 (2007).
47. D. Stramski, A. Bricaud, and A. Morel, "Modeling the inherent optical properties of the ocean based on the detailed composition of the planktonic community," Appl. Opt. **40**, 2929-2945 (2001).
48. D. R. Lide, "Physical and optical properties of minerals," in *CRC Handbook of Chemistry and Physics, 77th Edition*, (CRC Press, Boca Raton, Fla, 1997.) pp. 4.130–4.136.
49. L. Duforet, "Modelisation du rayonnement polarize dans une atmosphere absorbante et diffusante. Applications aux corrections atmosphériques au-dessus de l'océan," Ph.D. dissertation, 229 pp., Université du Littoral, France (2006).
50. M. S. Twardowski, E. Boss, J. B. Macdonald, W. S. Pegau, A. H. Barnard, and J. R. V. Zaneveld, "A model for estimating bulk refractive index from optical backscattering ratio and the implications for understanding particle composition in case I and case II waters," J. Geophys. Res. **106,** 14129–14142 (2001).
51. H. Loisel, X. Mériaux, J. F. Berthon, and A. Poteau, "Investigation of the optical backscattering to scattering ratio of marine particles in relation with their biogeochemical composition in the eastern English Channel and southern North Sea," Limnol. Oceanogr. **52**, 739-752 (2007).

1. Introduction

The absorption coefficients of phytoplankton and colored detrital matter, a_{phy} and a_{cdm}, respectively, as well as the backscattering coefficient of suspended particulate matter, b_{bp}, can now routinely be assessed from remote sensing measurements [1]. These coefficients provide information on new (compared to the chlorophyll concentration) biogeochemical components involved in oceanic carbon cycle studies such as particulate organic carbon (POC), etc. These space retrieved inherent optical properties (IOPs) allow to monitor the particulate and dissolved organic matter of the ocean surface. For example, the space retrieved particulate backscattering coefficient has been used to estimate the spatio-temporal variability of *POC* at local [2, 3, 4] and global scales [5]. In the same way, Siegel et al. [6] provided global distribution of colored detrital and dissolved material, *CDM*. Recent studies showed that information about the proportion between small-sized and larger particles [7], and about phytoplankton species [8, 9] and size [10, 11] may be assessed from satellite observations of

#94370 - $15.00 USD Received 28 Mar 2008; revised 22 May 2008; accepted 12 Jun 2008; published 11 Aug 2008

ocean color over the global ocean. Whereas all these advances open new doors in oceanic carbon cycle studies, information on the nature of the bulk particulate matter (for example, mineral vs. organic) from remote sensing is still missing. Moreover, most of these current inverse methods were essentially developed for open ocean waters, and their performance generally decreases in optically complex waters such as those found in coastal areas.

The inverse methods used to estimate such bio-optical information from space are based on different assumptions and mathematical developments. However, they all use the total remote sensing reflectance, $R_{rs}(\lambda)$ which is defined as the ratio of the upwelling radiance, $L_u(\lambda)$, to the downwelling irradiance, $E_d(\lambda)$, at different wavelengths λ, as input parameters (or a similar radiometric quantity):

$$R_{rs}(\lambda)=L_u(\lambda)/E_d(\lambda) \quad (1)$$

None of these models exploits the linear polarization of the upwelling light field from the ocean surface which can potentially be observed by an aircraft or a spacecraft. Many studies based on field measurements [12-15] as well as on theoretical or radiative transfer calculations [16-19] highlighted that the polarization of the underwater light field is sensitive to the nature of the suspended marine particles (for example phytoplankton vs. mineral). For example, Ivanoff et al. [12] stressed that the nature of particles suspended in water affects the relationships between the scattering coefficient and the degree of polarization, *P*. This latter parameter expresses the percentage of polarized light within the total radiation. Based on numerical radiative transfer simulations for the ocean-atmosphere system, previous investigators [18, 20] found that the polarized signal at red wavelengths may be used to discriminate phytoplankton from sediment particles. The directional and polarization information can also be used to significantly increase the efficiency of the IOPs inversion algorithms [21].

While the polarization of light is now extensively used in aerosol [22, 23] and cloud [24] remote sensing studies, it has never been exploited from space borne observations of ocean color, to our knowledge. This may partly be explained by the fact that the polarized water leaving radiation (i) only represents a small fraction of the total radiation recorded by the satellite sensor over open ocean waters and (ii) is fairly insensitive to marine constituents in open ocean waters [25]. However, over relatively bright areas, such as those encountered in coastal waters or during intense phytoplankton blooms, the polarized signal should be exploitable from remote sensing, at least at some appropriate wavelengths. In the present study, we examine the possibility of retrieving the polarized remote sensing reflectance, $R_{rs\text{-}p}$, simultaneously to the total remote sensing reflectance, R_{rs}, of oceanic surface layer from the POLarization and Directionality of the Earth's Reflectances (POLDER-2) sensor [26]. $R_{rs\text{-}p}$ is defined as the ratio of the polarized upwelling radiance to the downwelling irradiance. This study represents the preliminary step prior to the development of an algorithm based on space retrieval of the polarized remote sensing reflectance. Our purpose is to examine if $R_{rs\text{-}p}$ can be detected from satellite remote sensing measurement of ocean color, and if the behavior of the retrieved *P* values are consistent with expectations. For that purpose, two different areas are selected: the Rio de la Plata estuary waters dominated by suspended sediment, and the Barents Sea north of Norway during an intense phytoplankton bloom. The consistency of the results with previous field experiments, and with theoretical calculations as obtained from radiative transfer simulations, is analyzed.

2. Theoretical background

The scattered light is partially polarized according to the proportion defined by the degree of polarization:

$$P=(Q^2+U^2+V^2)^{0.5}/I, \quad (2)$$

#94370 - $15.00 USD Received 28 Mar 2008; revised 22 May 2008; accepted 12 Jun 2008; published 11 Aug 2008

where *I*, *Q*, *U* and *V* are the Stokes parameters [27]. The parameter *I* represents the intensity of light, whereas *Q* and *U* describe the linear polarization state, and *V* describes the elliptic polarization state. In the ocean, the linearly polarized radiation is generated through scattering of the penetrating sunlight. Elliptically polarized radiation can also be produced by the reflection under the sea-surface of the linearly polarized radiation [28]. However, the elliptic component is much less prominent than the linear one, and can be neglected in a good approximation [29, 30].

The degree of polarization of the ocean, $P(\theta)$, presents a bell-shaped distribution as a function of the scattering angle, θ. $P(\theta)$ generally reaches a maximum value around 90° and equals zero at the 0° and 180° scattering angles [31, 32]. Note, however, that the position of the maximum can change with the particle composition, i.e., the real part of the refractive index *n* and with the particle size distribution [Fig. 1(a-b)]. From *in situ* measurements, Ivanoff et al. [12] showed that the degree of polarization measured at a scattering angle of 90°, $P(90)$, decreases linearly with the scattering coefficient. In clear waters, the $P(90)$ values were found to be close to the maximum value measured for pure sea water (=0.84), whereas values as low as 0.10 were observed in eutrophic and turbid waters [12, 33]. The decrease of the degree of polarization from clear to turbid waters is mainly explained by multiple scattering events which contribute to depolarize the signal. Ivanoff et al. [12] pointed out that the dispersion observed around this decreasing trend could be related to the natural variability of the bulk suspended particle population. This assumption was confirmed by Mie theory calculations performed for homogeneous spherical particles with a size distribution approximated by a Junge-type hyperbolic model [31]. The degree of polarization increases with increasing Junge exponent ζ (i.e. with increasing the number of small particles relatively to larger ones), and with decreasing refractive index *n* [Fig. 1(c)]. Therefore, the examination of the relationships between the scattering (or backscattering) coefficient and the degree of polarization may bring complementary information on the nature of the particles.

#94370 - $15.00 USD Received 28 Mar 2008; revised 22 May 2008; accepted 12 Jun 2008; published 11 Aug 2008

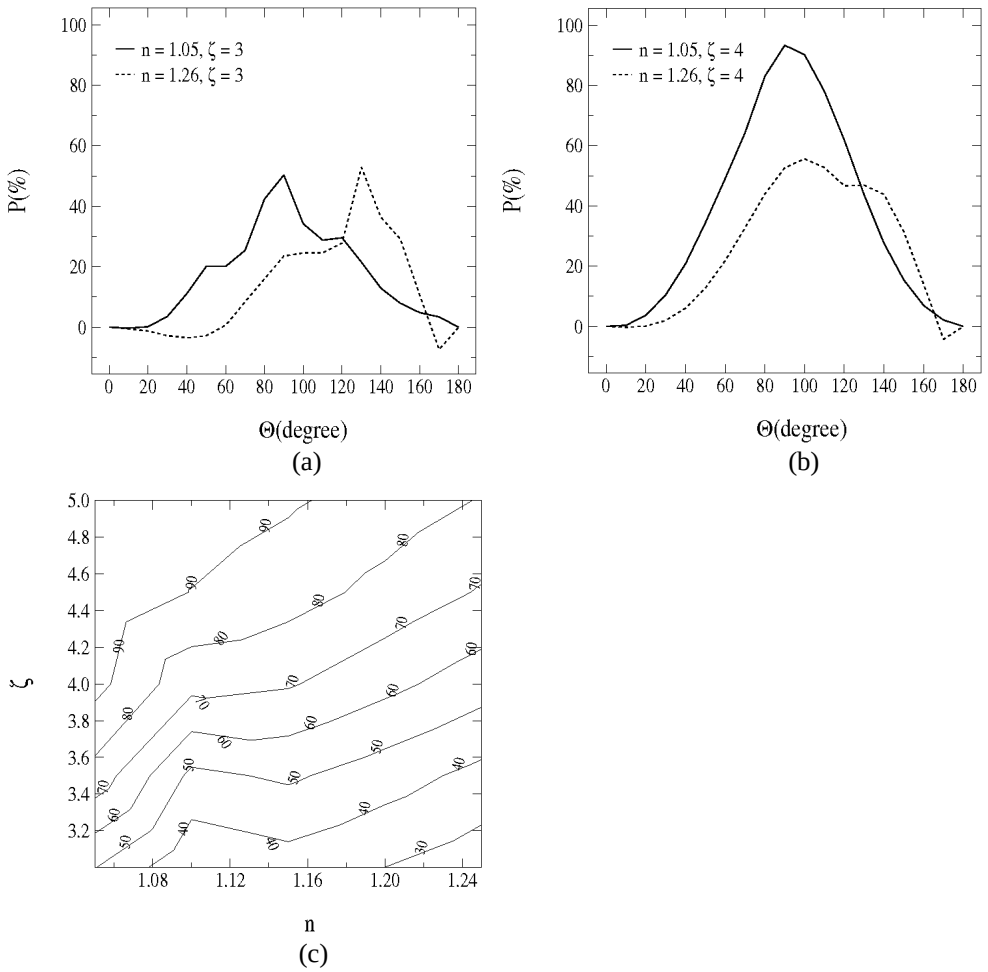

Fig. 1. Degree of polarization *P* (in %) as a function of the scattering angle, θ, for two extreme refractive index relative to waters, *n*, and for two different values of the PSD slope, ζ: a)ζ=3, and b) ζ =4. c) Contour diagrams of *P*(90) as a function of the parameters n (x-axis), and ζ (y-axis). Note that the *P* values presented in this figure are not affected by multiple scattering in contrast to what happens in the ocean.

3. POLDER-2 data processing

POLDER-2 is a wide field of view imaging radiometer which flew on ADEOS-2 from April to October 2003. The POLDER-2 instrument is a camera composed of a two-dimensional CCD detector array with a rotating wheel carrying spectral (443, 490, 565, 670, 763, 765, 865, and 910 nm) and polarized (443, 670, and 865 nm) filters [26]. For each polarized channel, the Stokes parameters are derived from measurements performed by using the same three spectral filters but with the polarized filter axes turned by steps of 60° [26]. Three polarized filters are then used to rebuilt the polarized signal for each polarized channel. In addition to the classical measurements and mapping characteristics of a narrow-band imaging radiometer, POLDER-2 has the unique ability to observe each pixel from 14 different viewing directions during a single satellite pass. Among the three available polarized channels, the red one, centered at 670 nm, is a good compromise for our study. Indeed, in contrast to the blue channel at 443 nm, it is much less affected by atmospheric (Rayleigh) scattering as well as by multiple scattering process occurring in the atmosphere-ocean system which depolarizes the signal. We

#94370 - $15.00 USD Received 28 Mar 2008; revised 22 May 2008; accepted 12 Jun 2008; published 11 Aug 2008

also disregarded the channel centered at 865 nm, due to the high sea water absorption value which considerably reduces the magnitude of the remote sensing reflectance.

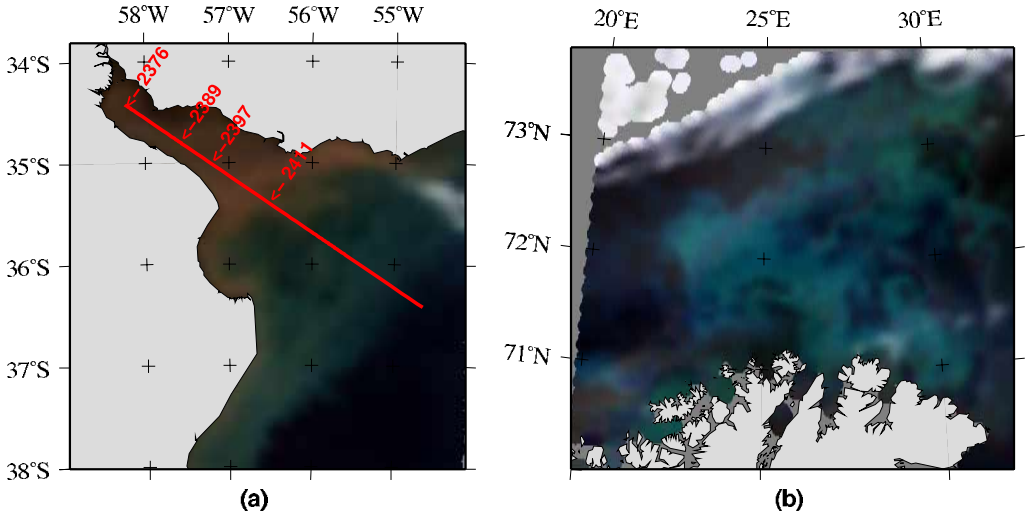

Fig. 2. POLDER2 selected scenes of RGB composites, over (a) the Rio de la Plata estuary (26 of May 2003), and (b) off Norway in the Barents sea (19 of July 2003). The red line in panel a corresponds to a transect specifically examined, and the numbers represent the pixel number (see text for details).

Two oceanic areas, characterized by different particulate matter composition, are selected: the Rio de la Plata estuary waters dominated by suspended sediments of terrestrial origin [Fig. 2(a)], and a phytoplankton bloom occurring offshore the Norway coasts in the Barents sea [Fig. 2(b)]. These scenes were chosen for their relatively high R_{rs} values at 670 nm, and their very clear sky conditions. This last point is essential since the correction for the aerosol effects on the top of atmosphere reflectance is still a very challenging task over eutrophic and turbid areas [34, 35]. Here, this correction is not necessary as the aerosol optical thickness at 670 nm of the surrounding black pixels is about 0.02 and 0.04 for the Rio de la Plata and the Barents sea images, respectively. Thus, the aerosol component can be considered as negligible in this study. For each selected scene, the top of atmosphere Stokes parameters (I, Q, U) recorded by the sensor in each viewing direction at 670 nm are corrected for Rayleigh scattering (using the measured surface pressure), for absorption by oxygen and water vapor (from ECMWF pressure and humidity profiles), and for ozone (as recorded by the Total Ozone Mapping Spectrometer sensor). The residual signal is then divided by the atmospheric diffuse transmission to obtain the above water Stokes parameters. For that purpose, the Rayleigh polarized radiance and the transmission are calculated using an atmospheric radiative transfer model developed by Duforet et al. [36]. This code accounts for the interface effects, which are modeled as a function of the sea surface wind speed value using the Cox and Munk's model [37]. The mean wind speed value (from ECMWF) is about 2 $m.s^{-1}$ and 5 $m.s^{-1}$ over the Barents Sea and Rio de la Plata areas, respectively. Note that the glitter contribution on the degree of polarization is negligible as the total and polarized reflectances are measured in (the) direction(s) far from the glitter pattern.

The values of P reported in this study are calculated from above water reflectance values, and are slightly different from those calculated from in water reflectance values, because of the transmission at the sea-air interface. On the basis of radiative transfer simulations, Kattawar and Adams [38], have shown that the P values calculated below the sea-air interface

#94370 - $15.00 USD Received 28 Mar 2008; revised 22 May 2008; accepted 12 Jun 2008; published 11 Aug 2008

are generally greater than those calculated above. Over a wide range of viewing angles this difference ranges between 5% and 25% for high (75°) and low (10°) sun zenith angles, respectively. The value of the sun zenith angle is 62° for the Rio de la Plata image, and 51° for the Barents sea image, which suggest that the effect of the interface is relatively small for our study. Furthermore, Chami and McKee [15] have recently shown that *P*, estimated from above water radiometric field measurements performed for sun zenith angles varying from 28° to 39°, is closely related to the biogeochemical properties of the marine particles in turbid environments.

4. Radiative transfer simulations

Radiative transfer calculations are conducted to verify the consistency of the POLDER-2 retrievals presented in this study, and especially the relationship between R_{rs} and *P*. These simulations are only performed for the Rio de la Plata image for which a reasonable assumption is that the inherent optical properties (IOPs) of the water are determined by pure sea water and sediments. In contrast, the Barents sea waters present much more variability in terms of IOPs due to the patchiness of phytoplankton biomass and the complex optical properties of the particles associated with the coccolithophores bloom (mostly due to the complex structure of the coccoliths, and of the variable concentration of detached coccoliths). Such complexity, which obviously impacts *P* and strongly affects the backscattering coefficient and then R_{rs} [39], makes the selection of input parameters for radiative transfer modeling purposes more difficult.

The radiative transfer equation is solved for the ocean-atmosphere system using the OSOA model which is fully described in [18]. This model is based on the successive orders of scattering method, and is able to predict the total and polarized signals in the coupled ocean-atmosphere system. The atmospheric parameters are those used for the POLDER-2 data processing and presented in the previous section. The simulations are carryied out for a homogeneous and infinitely deep ocean, for a flat sea surface, and in the absence of inelastic process. The inherent optical properties of marine constituents at 670 nm are modeled as follows. The absorption coefficient is considered to be totally dominated by pure sea water according to Pope and Fry [40]. The total and polarized particulate phase functions are computed by means of Mie theory. For that purpose two values of refractive index typical for sediments are considered: 1.15, and 1.20 (these values are relative to water). The particulate size distribution (PSD) is assumed to follow the Junge hyperbolic function with different Junge exponent values : -3.5, -4.0, and -4.5. The concentration of sediments varies between 0.5 to 60 $mg.l^{-1}$.

5. Results and discussion

5.1 The spatial distribution of R_{rs}, $R_{rs\text{-}p}$, and P

The spatial distribution of R_{rs}, $R_{rs\text{-}p}$, and *P* over the two selected areas are displayed in Fig. 3. These maps are obtained by averaging the directional values of each parameter over the different viewing directions. The mean and standard deviation values of the scattering angle are 135.95°±12.21° and 140.98°±10.46° over the Rio de la Plata estuary and the Barents sea, respectively. The total remote sensing reflectance images clearly reveal the plume and the bloom patterns [Fig. 3(a-b)]. At 670 nm, the variability of the total remote sensing reflectance, R_{rs}, is proportional to that of the particulate backscattering coefficient, b_{bp}, as the total absorption coefficient, *a*, is largely dominated by pure sea water absorption. Due to a much higher concentration of highly refractive suspended particles in water, the R_{rs} values are much higher for the Rio de la Plata Image (RPI) than for the Barents Sea Image (BSI). The concentration of suspended particulate matter, *SPM*, in the Rio de la Plata estuary is often greater than 50 $mg.l^{-1}$, with maximum values reaching 1 $g.l^{-1}$ [41]. For such *SPM* values, and assuming inherent optical properties values as those proposed by Doxaran et al. [42] for

#94370 - $15.00 USD Received 28 Mar 2008; revised 22 May 2008; accepted 12 Jun 2008; published 11 Aug 2008

different turbid estuarine waters, the R_{rs} values should range approximately between 0.025 to 0.060 sr^{-1}. This is consistent with the R_{rs} values obtained in RPI from POLDER2 [Fig. 3(a)]. The maximum R_{rs} values are observed at the frontal zone located at the inlet of the estuary, and are likely caused by strong resuspension effects due to the low bathymetry. For the Barents Sea Image, the R_{rs} values range between about 0 (the clearest waters) and 0.015 sr^{-1} [Fig. 3(b)]. Note that the pixels with R_{rs} values lower than the noise equivalent R_{rs} value, that is 0.0004 sr^{-1} [43], are not significant and only represent 3.6 % of the sea pixels. The relatively high R_{rs} values observed during this phytoplankton bloom are explained by the specific optical properties of the phytoplankton cells. The brightest blue color observed in Fig. 2(b) suggest the presence of coccolithophores which strongly backscatter light due to the calcium carbonate covering (coccoliths) surrounding their organic constituents.

Detached coccolithes of these phytoplankton cells also greatly contribute to increase the backscattering coefficient [44]. Smyth et al. [45] used satellite observations to study the occurrence of coccolithophore blooms in the Barents sea over a period of two decades. They showed from *in situ* measurements that the bloom occurring in July 2003 is of the coccolithophore species *Emiliana huxleyi*. Field radiometric measurements performed in a different area, but during a *Emiliana huxleyi* bloom confirm the range of remote sensing reflectance observed in our study [46].

Compared to R_{rs}, R_{rs-p} presents much lower values [Fig. 3(c-d)]. The R_{rs-p} values range between 0.001 and 0.012 sr^{-1} for RPI, and between 0 and 0.0035 sr^{-1} for BSI. Only R_{rs-p} values greater than 0.0009 sr^{-1} (the noise equivalent R_{rs-p} value) are significant [43], which represent 100% and 71.23% of the sea pixels for RPI and BSI, respectively. While the coefficient of variation (i.e. the ratio of standard deviation to the mean) of R_{rs-p} (40.6 %) is higher than that of R_{rs} (31.3%) for BSI, this is the reverse pattern for RPI (28.4 for R_{rs-p}, and 40.2 for R_{rs}). Comparison with *in situ* R_{rs-p} measurements is not discussed here as such measurements are still very rare, and generally presented in the literature in terms of degree of polarization [15]. Section 5.2 provides a comparison of the R_{rs-p} values estimated from POLDER-2, and those obtained from numerical simulations for the Rio de la Plata estuary.

#94370 - $15.00 USD Received 28 Mar 2008; revised 22 May 2008; accepted 12 Jun 2008; published 11 Aug 2008

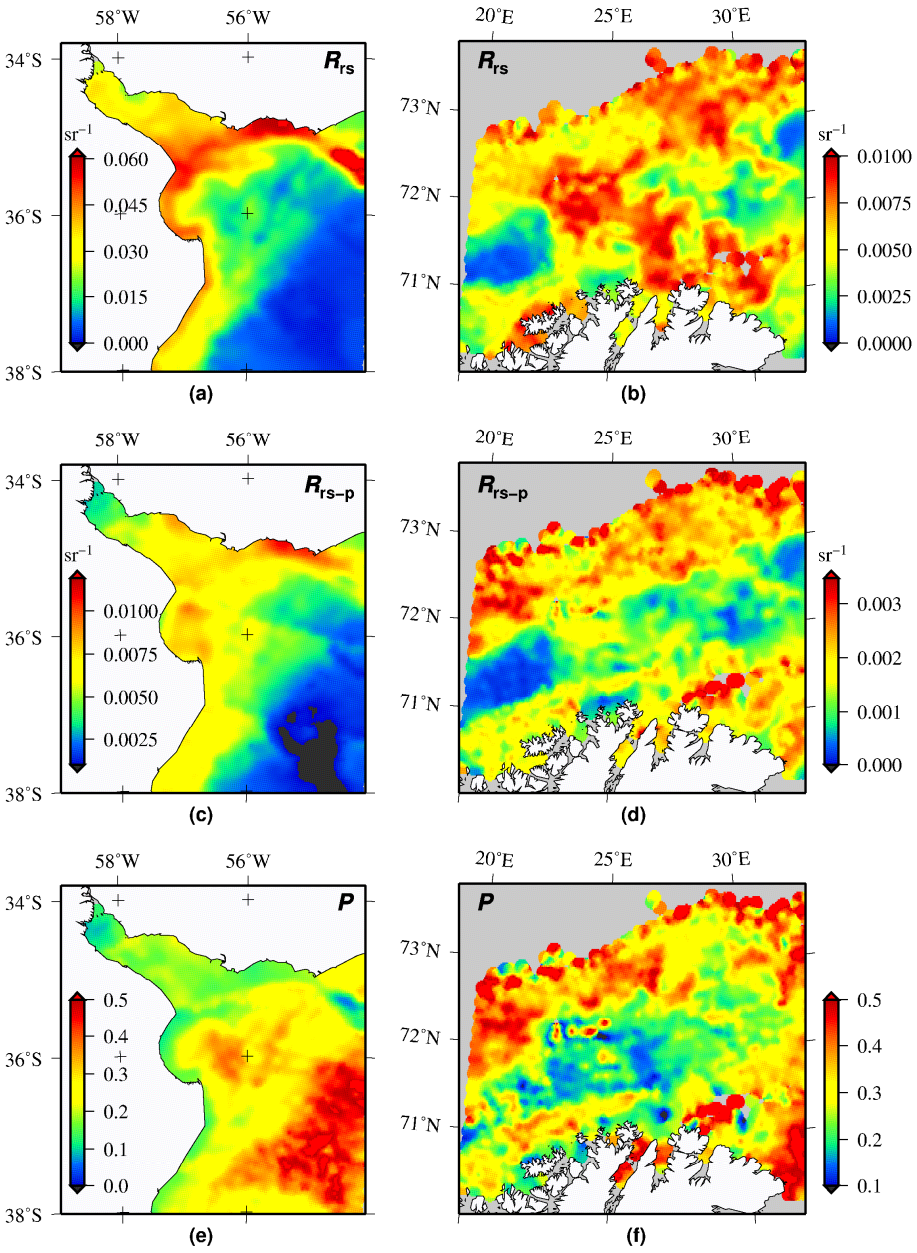

Fig. 3. Maps of R_{rs}, R_{rs-p}, and P at 670 nm for the Rio de la Plata estuary (left column), and the Barents Sea areas (right column).

The different R_{rs} and R_{rs-p} patterns directly impact the spatial distribution of the degree of polarization [Fig. 3(e-f)]. The general spatial pattern of P is roughly inversely proportional to that of R_{rs}. In RPI, the highest P values (~0.4) are observed offshore, and the lowest P values (~0.05) are found at the inlet of the estuary after the frontal zone. This pattern is consistent with expectation as P should decrease from clear to more turbid waters. The spatial pattern of

#94370 - $15.00 USD Received 28 Mar 2008; revised 22 May 2008; accepted 12 Jun 2008; published 11 Aug 2008

P in BSI is much less organized than in RPI. The *P* values for BSI ranges from 0.1 to 0.5, with a coefficient of variability of 35.6 (against 53.2 for RPI).

5.2 Examination of the origin of the variability of P

The *P* variability reflects changes in the scattering angles, turbidity (i.e. contribution of the multiscattering effects), and nature of the suspended marine particles (i.e size, shape, and refractive index). Direct interpretation of the different spatial patterns of *P* (Fig. 3), in terms of biogeochemical properties of marine particles should then be considered with caution, even qualitatively. The impact of the different factors responsible for the variability of *P* are now examined separately.

The evolution of R_{rs}, $R_{rs\text{-}p}$, and *P* is analyzed along a transect in the Rio de la Plata which extend from the inner part of the estuary to offshore waters (Fig. 4). Its exact location is given in Fig. 2(a). The value of the scattering angle along this transect remains roughly the same (138° ± 2°), which points out that the variations of R_{rs}, $R_{rs\text{-}p}$, and *P* are essentially governed by the turbidity and the water composition (Fig. 5). As already noticed in Fig. 3, R_{rs} and $R_{rs\text{-}p}$ exhibit almost the same spatial evolution, however with an opposite trend between pixels 2376 and 2381 where R_{rs} decreases by a factor of 1.3 while $R_{rs\text{-}p}$ increases by the same factor. This may be explained by a large increase of *P* (by a factor of 1.7), probably due to a great variability of the suspended particulate assemblage between these two locations. The degree of polarization shows slight fluctuations around the mean value of 0.18 ± 0.03 from pixel 2376 to 2411 (that is about 245 km), and then sharply increases by a factor of 2.1 up to the end of the transect (where both R_{rs} and $R_{rs\text{-}p}$ decrease). Some interesting features can be noticed at some certain locations where *P* exhibits significant variations for the same R_{rs} value (i. e. same scattering level). For example, *P* varies by a factor of 1.5 between pixels 2377 and 2389, whereas R_{rs} is constant (0.034 sr^{-1}). Similar observation can be done between pixels 2391 and 2397, where R_{rs} varies only by a factor of 1.02, whereas *P* increases by a factor of 1.21. This behavior can be attributed to variations in the particulate assemblage between these locations.

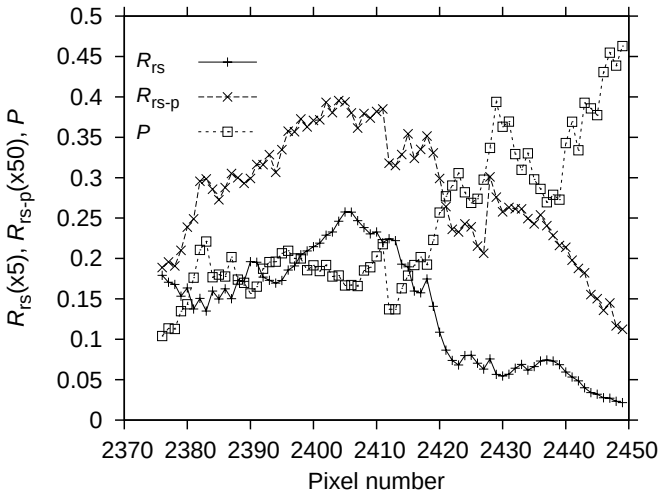

Fig. 4. Evolution of R_{rs}, $R_{rs\text{-}p}$, and *P* along a transect in the Rio de la Plata estuary (represented by the red line in Fig. 2a).

The differentiation of the three main phenomena involved in the variability of *P*, that is its angular dependence, the turbidity, and the particulate assemblage characteristics, may be assessed by looking at the evolution of R_{rs} as a function of *P* for a restricted range of

#94370 - $15.00 USD Received 28 Mar 2008; revised 22 May 2008; accepted 12 Jun 2008; published 11 Aug 2008

scattering angles (Fig. 5). The average value and standard deviation of the scattering angle considered in Fig. 5 is 130°±1° for both scenes. Because the R_{rs} variability at 670 nm is mainly driven by the particulate backscattering, this figure is somewhat similar to that presented by Ivanoff et al. [12], between the scattering coefficient at 90°, and *P*.

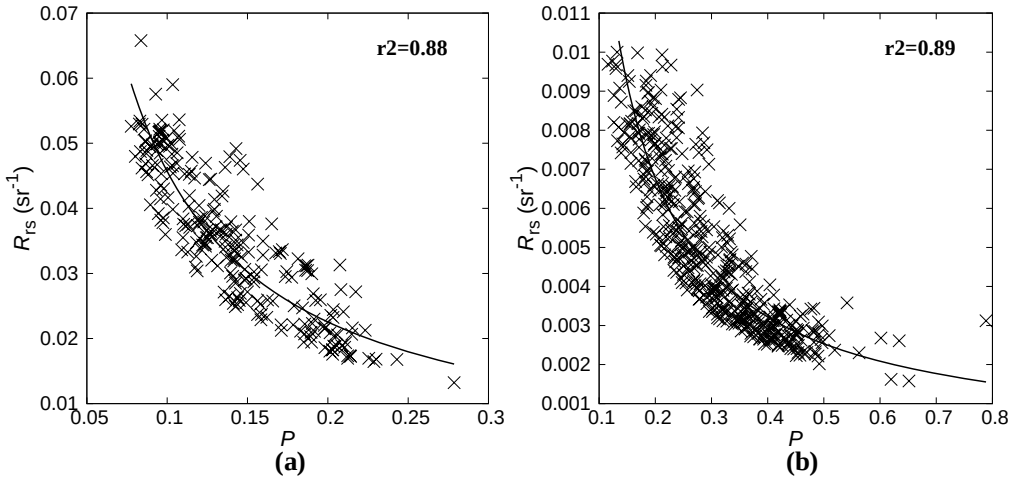

Fig. 5 Scatter plot of R_{rs} as a function of *P* at 670 nm for (a) the Rio de la Plata estuary, and (b) the Barents Sea areas. The black lines in panel a and b correspond to the fits described by the equations 2 and 3, respectively. The square correlation coefficient (r^2) is given. Note the different scales of the two panels.

The net decreasing of *P* with increasing R_{rs}, due to the multiple scattering effects, is clearly evidenced over the two different areas. Such a decreasing trend has also been reported by Chami and McKee [15] between *P* measured at the Brewster viewing angle and the concentration of the suspended particulate matter (which controls the value of $R_{rs}(670)$, to first order). An exponential function can be fitted between *P* and R_{rs} for RPI (Eq. (3)) and BSI (Eq. (4)), in good agreement with the results of Ivanoff et al. [12]:

$$P = 0.0099\ R_{rs}^{(-0.768)} \qquad (r^2=0.88) \qquad (3)$$

$$P = 0.0054\ R_{rs}^{(-0.739)} \qquad (r^2=0.89) \qquad (4)$$

These two relationships present very similar exponential slopes, but their offset (in linear scale) remarkably differ: for the same R_{rs} value, *P* is higher by almost a factor of 2 for the Rio del Plata estuary, than for the Barents sea. Assuming that this effect is only attributable to the nature of the suspended marine particles, this result suggests that the bulk particulate assemblage is dominated by relatively larger particles with higher refractive index in BSI than in RPI. While relatively large phytoplankton cells are expected during the bloom of *Emiliana huxleyi* occurring in the Barents sea, the refractive index of these cells (*n*=1.05, [47]) and of their associated detached coccoliths (*n*=1.19, [48]), have generally (depending on the concentration of detached coccoliths in waters) a lower refractive index than that of mineral particles from terrigenous origin (*n*=1.14-1.26, [49]). However, based on numerical Mie computations it is shown that *P* is much more sensitive to size than refractive index for this range of refractive index and scattering angles. Indeed, the isolines plotted in Fig. 1(c) for θ=90° tend to be much more parallel to the abscissa (i.e. to the refractive index) when the scattering angles increases [50]. This difference could also partly be explained by a higher

#94370 - $15.00 USD Received 28 Mar 2008; revised 22 May 2008; accepted 12 Jun 2008; published 11 Aug 2008

concentration of dissolved and particulate absorbing material in RPI than in BSI, which may make RPI waters more single scattering dominated than BSI waters.

For this narrow range of scattering angle, a relatively large dispersion of the data is observed around the mean exponential trends. *P* can vary up to a factor of 1.5 for a given R_{rs} value over the two studied areas. A higher dispersion is generally observed over the Barents sea area than over the Rio de la Plata estuary. The coefficient of variability is 41% and 31% for BSI, and RPI, respectively (note that it was the reverse pattern when all scattering angles were considered in Fig. 3). Assuming that such dispersion is due to the particulate assemblage variability [12, 31], this suggests that the nature of the bulk particulate matter is more variable over the Barents Sea area than over the Rio de la Plata estuary (at least for these two images).

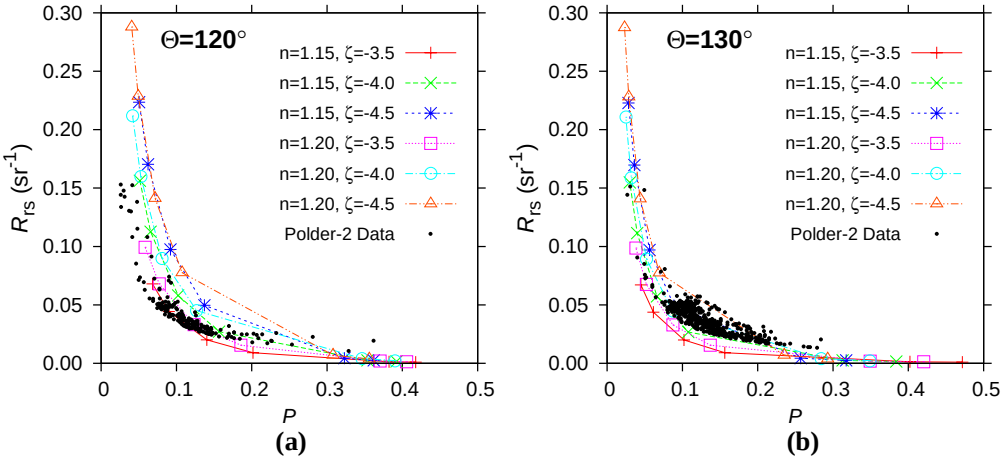

Fig. 6. Variation of R_{rs} as a function of *P* for the value of the scattering angle of (a) 120° and (b) 130° for the Rio de la Plata estuary waters. The colored symbols represent data obtained from the radiative transfer simulations performed for different values of the refractive index, *n*, and PSD slope, ζ, as indicated. The black dots represent the data obtained from POLDER-2 observations. Note that the *P* values are lower than those presented in Fig. 1 for which the calculations did not account to multiple scattering.

The relationship between R_{rs} and *P*, as revealed from the POLDER-2 observations, is evaluated for the Rio de la Plata image by the means of radiative transfer calculations carried out as described in section 4. The results of these numerical computations are superimposed on the POLDER-2 data for θ=120° [Fig. 6(a)], and θ=130° [Fig. 6(b)]. The evolution of *P* as a function of R_{rs} obtained from these radiative transfer simulations is in excellent agreement with the POLDER-2 observations. The hyperbolic trend observed between *P* and R_{rs} from POLDER-2 is well confirmed in both shape and amplitude from the radiative transfer simulations. For a given scattering angle, each variation of the refractive index and of the slope of the particle size distribution affects the *P* vs. R_{rs} relationship, likely contributing to the observed scatter in POLDER-2 data. For example, for θ=120° and R_{rs} = 0.06 sr^{-1}, the increase of the degree of polarization by a factor of 1.6 observed from POLDER-2 in RPI is coherent with an increase of the PSD slope from –3.5 to –4. According to these results, it could be tempting to retrieve information about the particles assemblage (*n* and ζ) by examining the relationship between R_{rs} and *P*. However, it should be done with caution as modifications of *n* for the same PSD slope does not necessarily modify the R_{rs} vs. *P* relationship (Fig. 6). This is in agreement with Mie calculations which showed that, for such scattering angles, *P* is much more sensitive to ζ than n [50]. Further theoretical and experimental investigations are obviously needed at this point. The effect of the particle shape on *P* should also be examined.

#94370 - $15.00 USD Received 28 Mar 2008; revised 22 May 2008; accepted 12 Jun 2008; published 11 Aug 2008

6. Concluding remarks

This preliminary study shows that polarized radiations of the natural light scattered back out of the ocean can be extracted from satellite observations of ocean color at least over bright oceanic areas. The absolute values of the polarized remote sensing reflectance and of the degree of polarization are consistent with expectations, and with previous theoretical and experimental findings. Our confidence in our P retrieval from POLDER-2 is reinforced by the examination of the behavior between R_{rs} and P which is similar to in-situ observations made by Ivanof et al. [12] and Chami and McKee [15]. Comparisons with numerical simulations performed for the ocean-atmosphere system are also provided for the Rio de la Plata estuary. These radiative transfer simulations, performed for different physical characteristics of suspended marine particles, confirm that the scatter of the POLDER-2 data observed around the hyperbolic trend between R_{rs} and P may be explained by the variability of the bulk particulate assemblage composition.

The present study has been conducted for two idealized cases (no aerosols) to assess the feasibility of extracting water polarized radiations from remote sensing over bright areas. Prior to any generalization of these results two main studies should be conducted. First, the sensitivity of the effect of the presence of aerosols should be investigated. Atmospheric corrections over turbid waters, necessary to accurately assess the total remote sensing reflectance and a fortiori the polarized remote sensing reflectance, are still very challenging. Once good atmospheric corrections schemes are available for such waters, comparison with other bio-optical products derived from ocean color observations and related to the nature of the marine particles in suspension should be performed. Secondly, *in situ* measurements of the polarized remote sensing reflectance, which are still very rare, should be performed in biogeochemically contrasted waters. The behavior of P should then be compared to other bio-optical proxy usually used *in situ* to characterize the bulk particulate assemblage, such as the particulate backscattering to scattering ratio [51, 52].

Acknowledgments

This work was supported by Centre National d'Etude Spatiale (CNES) and Région Nord Pas-de-Calais through the doctoral fellowship of Lucile Duforet, and by Centre National de la Recherche Scientifique in the frame of the PNTS program. POLDER-2 ocean color data are provided by CNES. We thank Cyril Moulin, Jean-Marc Nicolas, and Jean-Luc Deuzé for their guidance during the POLDER-2 data processing. The authors thank two anonymous reviewers for their relevant comments.

#94370 - $15.00 USD Received 28 Mar 2008; revised 22 May 2008; accepted 12 Jun 2008; published 11 Aug 2008